Molecular Vision 1998; 4:20 <http://www.molvis.org/molvis/v4/p20>
Received 19 June 1998 | Accepted 25 September 1998 | Published 6 October 1998

© Molecular Vision

GLC1A mutations point to regions of potential functional importance on the TIGR/MYOC protein

Frank W. Rozsa,[1] Satoko Shimizu,[1] Paul R. Lichter,[1] A. Tim Johnson,[1] Mohammad I. Othman,[1] Kathleen Scott,[1] Catherine A. Downs,[1] Thai D. Nguyen,[2] Jon Polansky,[2] Julia E. Richards[1,3]

[1]Department of Ophthalmology, The University of Michigan Medical School, Ann Arbor, MI, USA; [2]Department of Ophthalmology, The University of California at San Francisco, CA, USA; [3]Department of Epidemiology, The University of Michigan School of Public Health, Ann Arbor, MI, USA

Purpose: The aim of this study was to screen affected members of glaucoma families for mutations in the Trabecular Meshwork Inducible Glucocorticoid Response (*TIGR*) gene also known by the name myocilin (*MYOC*) or by combined names such as *TIGR/MYOC*. Our primary objectives were (1) to identify mutations responsible for glaucoma in members of three families for which we have shown linkage between chromosome 1 *GLC1A*-region markers and the primary open angle glaucoma (POAG) phenotype, and (2) to determine the relationship of these and other mutations to key points of predicted function and structure of the TIGR/MYOC protein.

Methods: DNA sequence determination was used to identify sequence changes in sections of the *TIGR/MYOC* gene that were PCR-amplified from genomic DNA from the probands of three previously-reported *GLC1A* juvenile-onset POAG families, UM:JG1, UM:JG3, UM:GL57, and unmapped family UM:JG5. Allele-specific oligonucleotide hybridization was used to screen for the identified mutations in PCR-amplified DNA from individual members of each pedigree and from a panel of 11 additional juvenile glaucoma family probands, 42 adult POAG family probands, and 43 normal individuals. Computerized algorithms were used to identify functional motifs and predict structures of normal and mutant forms of the protein.

Results: Sequence changes were found that alter amino acids in the olfactomedin-like domain near the carboxy terminal end of the TIGR protein in affected members of families UM:JG1 (Pro370Leu), UM:JG3 (Val426Phe), UM:GL57 (Glu323Lys) and UM:JG5 (Gly252Arg). Co-segregation of glaucoma and Pro370Leu, Val426Phe, and Gly252Arg in known *GLC1A* families suggests that these are mutations. Although the Gly252Arg substitution observed in UM:JG5 is non-conservative, it was not possible to distinguish whether it is a mutation or a polymorphism. None of the sequence changes described in these families were observed in other juvenile glaucoma cases in this study, nor in any of the POAG or phenotypically normal individuals tested here. Analysis of amino acid sequence changes resulting from mutations described in this and other works demonstrate localization of many mutations in the vicinity of predicted functional motifs in the olfactomedin-like domain. Identification of rat latrophilin (LPH1/CIRL) as a new member of the olfactomedin-like protein family to which TIGR/MYOC belongs suggests that the region of olfactomedin homology is a protein domain that can occur in different protein contexts.

Conclusions: Location of mutations described in this and previous work suggests that some specific predicted protein motifs in the olfactomedin-like domain may be important to TIGR/MYOC function. In some cases, the role of TIGR/MYOC in the etiology of glaucoma may result from alteration of the sequences recognized by modifying enzymes such as casein kinase II. In other cases altered protein folding may affect access of enzymes to their target sequences on TIGR/MYOC. Although modifications and structures discussed here are predicted rather than proven, they provide a useful theoretical framework for design of subsequent experiments. Alterations to protein folding and predicted modification motifs cannot explain the pathogenic mechanisms of all of the known *TIGR/MYOC* glaucoma mutations.

Beginning with the 1993 report by Sheffield et al. that mapped the first primary open angle glaucoma (POAG) gene *GLC1A* to 1q23-q31 [1], a total of six POAG loci have been mapped, including *GLC1B*, *GLC1C*, *GLC1D*, *GLC1E*, and *GLC1F* [2-6]. Subsequent reports by other groups [7-12] confirmed the original *GLC1A* map location and gradually reduced the physical and genetic interval containing the gene, while also providing specific information on the clinical phenotype of individuals affected with *GLC1A* glaucoma [12-14]. Previously-published *GLC1A* juvenile-onset (JG) families show similar phenotypic expression, including similarities in levels of elevation of intraocular pressure (IOP) and the age at diagnosis of POAG [14]. Glucocorticoid-induced human trabecular meshwork (HTM) cells have time course and dose response patterns of expression of the trabecular meshwork inducible glucocorticoid response (TIGR) protein similar to the time course and dose response of subjects who demonstrate corticosteroid-induced elevation of IOP [15-17]. By exploiting this observation, Nguyen and colleagues used differential screening with cDNA probes from dexamethasone-induced and uninduced HTM cells to screen a cDNA library prepared from dexamethasone-induced HTM cells [18]. The result of that screening was a cDNA that encodes the TIGR protein, which was subsequently named myocilin (MYOC) when cloned from retina by Kubota and colleagues [19,20]. *TIGR/*

Correspondence to: Julia E. Richards, Department of Ophthalmology, W. K. Kellogg Eye Center, University of Michigan, 1000 Wall Street, Ann Arbor, MI, 48105; email: richj@umich.edu. Dr. Johnson is now at the Department of Ophthalmology, The University of Iowa Hospitals and Clinics, Iowa City, IA, USA

MYOC transcripts have also been observed in ciliary body, iris, heart, skeletal muscle, stomach, thyroid, trachea, bone marrow, thymus, prostate, small intestine and colon [19,21-23]. Expression of *TIGR/MYOC* has also been observed in glaucomatous native HTM tissue using immunohistological approaches [24].

Stone and colleagues [25] identified *TIGR/MYOC* mutations in cases of *GLC1A* glaucoma, including members of the original juvenile glaucoma family used to map the *GLC1A* locus [1] and in members of the general glaucoma population [25,26]. Associations between other *TIGR/MYOC* mutations and *GLC1A*-linked glaucoma have subsequently been observed by other groups [22,27-29]. Most mutations identified in the *TIGR/MYOC* gene are missense mutations in the olfactomedin-like domain contained on *TIGR/MYOC* exon 3, only some of which co-segregate with glaucoma. Polymorphisms that are silent have been reported as well as polymorphisms that alter the TIGR/MYOC amino acid sequence, but their role in glaucoma has not yet been determined. In some instances, specific *TIGR/MYOC* mutations have been shown to be associated with severe glaucoma with early age of onset, suggesting that a critical region for the normal function of TIGR/MYOC has been altered [22,27].

In this paper we present three different *TIGR/MYOC* missense mutations that co-segregate with POAG in our previously reported *GLC1A* juvenile glaucoma families UM:JG1, UM:JG3, UM:GL57 [7,14,30] plus another TIGR/MYOC amino acid substitution in a previously unmapped juvenile glaucoma family UM:JG5. Two previously-observed *TIGR/MYOC* polymorphisms are also presented. The observed amino acid substitutions from this and other studies are discussed relative to predicted protein structures and protein modification sites.

METHODS

Patient and Family collection— Clinical descriptions and linkage studies of families UM:JG1, UM:JG3, and UM:GL57 were previously reported [7,14,30]. Pedigrees are shown in Figure 1. Glaucoma locus assignment had not previously been made for families UM:JG5 and UM:GL7, which are too small for use in linkage studies. Four additional members of UM:JG1 were subsequently examined with the use of tests and diagnostic criteria as previously reported [7]. All patients underwent complete ophthalmological examinations consisting of slit-lamp biomicroscopy, optic disk examination, IOP measurement by applanation, refraction, gonioscopy and visual field assessment. Criteria for glaucoma diagnosis were elevated IOP >20, 23, 24 mm Hg for UM:JG1, UM:GL57, and UM:JG3, respectively with characteristic optic disk damage and/or visual field loss. In the absence of optic disk and visual field damage individuals with IOP > 30 mm Hg were classified affected. Clinical data for pedigrees with mutations in *TIGR/MYOC* in this work are shown in Table 1. Genomic DNA was isolated from whole blood using a Puregene DNA Isolation Kit (Gentra Systems, Research Triangle Park, NC) according to the manufacturers protocol.

Polymerase Chain Reaction (PCR) amplification of TIGR/MYOC gene fragments— Regions to be sequenced were amplified from genomic DNA using an AmpliTaq Gold PCR kit (Perkin-Elmer, Foster City, CA) with an annealing temperature of 55 °C (see Table 2 for primers). Fragments were isolated from low melt agarose gels followed by

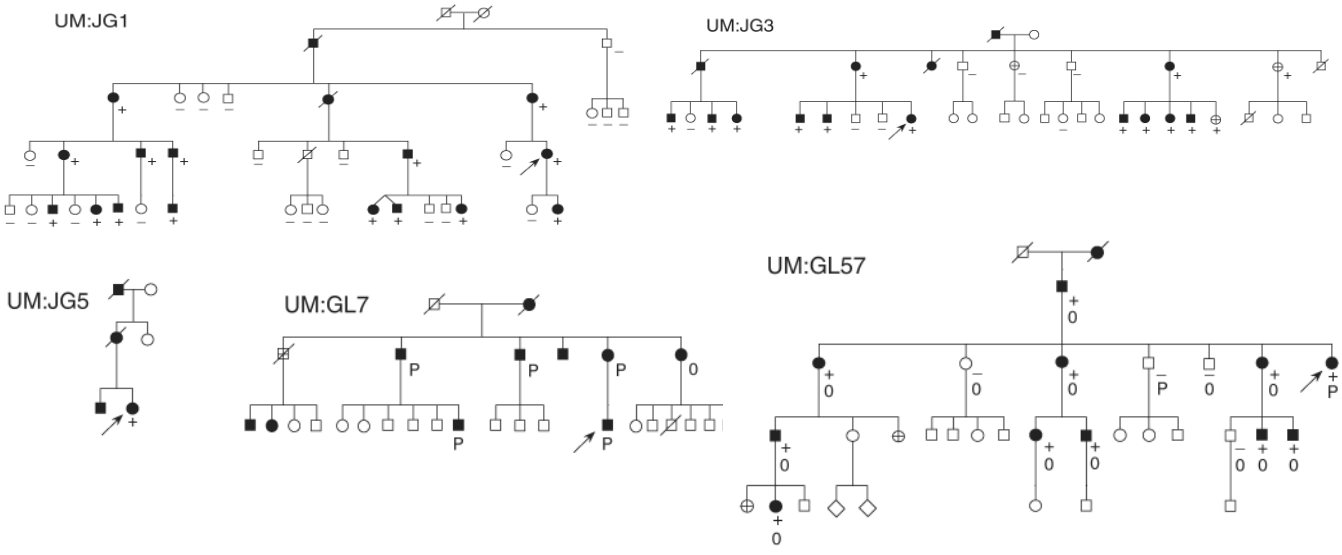

Figure 1. Pedigrees of five families screened for mutation in the *TIGR/MYOC* gene. Pedigrees include screened subjects and their first degree relatives. Generations consisting of individuals too young to determine the glaucoma phenotype are not shown. Males and females are indicated by squares and circles, respectively. Deceased members are indicated with a diagonal line through symbol. Individuals affected with glaucoma are indicated with filled symbols. Individuals whose glaucoma status or sex was indeterminate are indicated with a crosshatch inside the symbol or by diamonds, respectively. Individuals containing or lacking a co-segregating mutation identified in the proband are indicated by (+) or (-), respectively. Individuals in UM:GL7 and UM:GL57 containing or lacking a polymorphism are identified by (P) or (O), respectively.

extraction of the melted gel with equal volumes of phenol followed by ethanol precipitation. The purified fragments were then used as templates for DNA sequence determination or immobilized on Hybond N+ nylon membrane (Amersham, Arlington Heights, IL) for allele specific oligonucleotide (ASO) hybridization.

DNA sequencing— Direct sequencing of PCR-amplified fragments of the *TIGR/MYOC* gene was carried out with an AmpliCycle Sequencing Kit (Perkin-Elmer) according to the manufacturers protocol. Sequencing reactions used γ-^{33}P end labeled primers (Table 2) and an annealing temperature of 57 °C. Samples were size fractionated by electrophoresis on a 6% denaturing polyacrylamide sequencing gel. In addition, some PCR fragments from families UM:JG5 and UM:GL57 were sequenced with the use of a dye-terminator cycle sequencing kit (Perkin-Elmer) and analyzed on an ABI377 semi-automated sequencer. Sequence similarity comparisons were carried out using BLAST (National Center for Biotechnology Information) to search the Swiss-Prot and GenBank/EMBL databases. PILEUP (Genetics Computer Group, Madison, WI) was used to carry out sequence alignments. The codon numbering system used here is based on the revised GenBank entry U85257 and differs from numbering in Stone et al [25].

Screening by allele specific oligonucleotide (ASO) hybridization— One pair of oligonucleotides was constructed for each new *TIGR/MYOC* allele in families UM:JG1, UM:JG3, UM:JG5, and UM:GL57, with the central nucleotide containing either the altered or the normal base from the *TIGR/MYOC* sequence (Table 2). Melting temperatures for oligonucleotides were calculated using the formula of Bolton and McCarthy [31]. Oligonucleotides were end-labeled by transfer of ^{32}P from γ-^{32}P dATP (Amersham) using T4 polynucleotide kinase (New England Biolabs, Beverly, MA). Fragment I was amplified by PCR from genomic DNA to screen for the Pro370Leu, Val426Phe and Tyr347Tyr mutations present in UM:JG1, UM:JG3, UM:GL57, respectively (Table 2, Figure 2). Similarly, Fragment J was screened for the Gly252Arg mutation in UM:JG5 (Table 2, Figure 2). Screening was performed on members of each probands family and a test panel consisting of 43 normal individuals of ages 35 to 83 years (mean 55 years), 11 unrelated JG individuals with POAG diagnosed prior to age 35, and 43 individuals with POAG diagnosed after age 35. PCR-amplified DNA was bound to Hybond N+ (Amersham) membrane under alkaline denaturing conditions and fixed to the membrane using a Stratalinker UV lightsource (Stratagene, La Jolla, CA). Blots were prehybridized for 60 min at 47 °C in 5 x SSPE, pH7.4 (0.75 M NaCl, 50 mM NaH_2PO_4, 5 mM EDTA), 5 x DET (0.1% polyvinylpyrrolidone, 0.1% ficoll, 0.1% BSA, 1 mM Tris-HCl pH8.0, 1 mM EDTA), 0.5% sodium dodecyl sulfate (SDS) with 100 µg/ml salmon sperm DNA. Following prehybridization, the ^{32}P-end labeled mutant oligonucleotide was added for 60 min at 47 °C with gentle agitation. Non-specific label was removed by sequential 10 minute washes in: 2 x SSPE, 0.1% SDS at 25 °C; 5 x SSPE, 0.1% SDS at 52 °C; and 2 x SSPE, 0.1% SDS at 58 °C. The blot was briefly air-dried and exposed to film, after which the blot was stripped using 0.4 N NaOH at 42 °C for 30 minutes, neutralized with 0.1 x SSC (15 mM NaCl, 16.5 mM NaCitrate), 0.1% SDS, 0.2 M Tris-HCl pH7.5 at 42 °C for 30 minutes, and rehybridized with the normal oligonucleotide under the same conditions.

Screening by restriction digest— Templates for AlwNI restriction digests were prepared by PCR amplification to generate Fragment K (Table 2, Figure 2) from the UM:JG1 and UM:GL7 pedigrees and the test panel described above. Likewise, Fragment L was amplified from members of the UM:GL57 pedigree and test panel to screen for the Glu323Lys mutation using BsrI (Table 2, Figure 2). PCR products were digested for two hours at either 37 °C (AlwNI) or 65 °C (BsrI) using the manufacturers buffer (New England Biolabs). Restriction fragments were separated on either 1% agarose or 3.5% Nusieve agarose (FMC, Rockland, ME) gels for the AlwNI and BsrI digestions, respectively.

Secondary structure predictions— The protein sequences for TIGR/MYOC and its sequence variants were analyzed with the Genetyx-Mac 9.0 program (Software Development LTD, Japan) program using the predictive algorithms by Chou-Fasman [32] and Garnier, Osguthorpe, and Robson [33,34]. Protein motifs in TIGR/MYOC were identified from the Blocks [35], Prints [36] and Prosite [37] databases using the Blocks Searcher, FingerPrintScan, and ScanProsite programs,

Table 1. Clinical Data for five Juvenile-onset and one Mixed-onset Glaucoma Families

Pedigree	UM:JG5	UM:GL57	UM:GL7	UM:JG1	UM:JG3	UM:JG2
Ethnicity	Caucasian	Panamanian	African-American	Caucasian	Caucasian	Caucasian
Glaucoma type	Juvenile	Juvenile	Mixed	Juvenile	Juvenile	Juvenile
Age at diagnosis (yr)						
Mean	26	19	52	12	26	18
Range	NA	9-43	29-71	5-27	16-46	4-26
Maximum IOP (mm Hg)						
Mean	62	43	27	45	43	42
Range	NA	23-59	22-38	25-66	32-52	24-45
Mutation Identified in Proband	Gly252Arg	Glu323Lys Tyr347Tyr	Thr325Thr	Pro370Leu	Val426Phe	Ile477Asn

Table 2. Oligonucleotides used for PCR, Sequencing, and ASO in this work. Table 2A. Primers sets used to amplify *TIGR* exons for sequencing. Table 2B. Primer sets used to amplify *TIGR* fragments for ASO and restriction analysis. Table 2C. Oligonucleotides used to sequence mutations. Table 2D. Oligonucleotides used for ASO hybridization.

2A.

Forward	Reverse	Family	Use	Fragment
5' GCTTTCCAGAGGAAGCCTCACC	5' CTCCAGAACTGACTTGTCTC	All	Exon 1	A
5' AATTGACCTTGGACCAGG	5' CACTGGCCCCTTCTCAGCCTTGCT	All	Exon 1	B
5' GCGACTAAGGCAAGAAAATG	5' AGGTCACTACGAGCCATATC All	All	Exon 1	C
5' ACATAGTCAATCCTTGGGCC	5' ATGAATAAAGACCATGTGGG	All	Exon 2	D
5' GGATTAAGTGGTGCTTCG	5' GCATAAACTGGCTGATGAG	All	Exon 3	E
5' AATTACTGGCAAGTATGGT	5' CAATGTCCGTGTAGCCAC	All	Exon 3	F
5' GGGTGCTGTGGTGTACTC	5' CATGCTGCTGTACTTATAGCG	All	Exon 3	G
5' GAACTCGAACAAACCTGGGAG	5' GAGCTATTCTGCTTCCT	All	Exon 3	H

2B.

Forward	Reverse	Family	Use	Fragment
5' AAGGTTCACATACTGCCTAG	5' GAAAGCAGTCAAAGCTGCC	JG1	ASO	I
		JG3	ASO	I
		GL57(P)	ASO	I
5' CTGGCTCTGCCAAGCTTCCGCATGA	5' GGCTGGCTCTCCCTTCAGCCTGCT	JG5	ASO	J
5' AATTACTGGCAAGTATGGT	5' CATGCTGCTGTACTTATAGCG	JG1	AlwNI	K
		GL7	AlwNI	K
5' CACCCAGGAGACCACGTGGAGAATC	5' GAGGCCTGCTTCATCCACAGCCAAG	GL57(M)	BsrI	L

(P): Tyr347Tyr polymorphism in UM:GL57; (M): Glu323Lys mutation in UM:GL57

2C.

Oligonucleotide	Family	Use	Fragment
5' GGGTGCTGTGGTGTACT	JG1	Sequence	I
5' TTGGCTGTGGATGAAGCA	JG3	Sequence	I
5' CTGGCTCTGCCAAGCTTCCGCATGA	JG5	Sequence	J
5' AATTACTGGCAAGTATGGT	GL7	Sequence	K
5' AAGGTTCACATACTGCCTAG	GL57(P)	Sequence	I
5' TATGACAGTTCTGGACTCAGC	GL57(M)	Sequence	L

(P): Tyr347Tyr polymorphism in UM:GL57; (M): Glu323Lys mutation in UM:GL5

2D.

Oligonucleotide	Name	Family	Use	Fragment
5' GACAGTTCCCGTATTCTTG	370PRO	JG1	Control	I
5' GACAGTTCCTGTATTCTTG	370LEU	JG1	Mutant	I
5' AAGCAGTCAGTCGCCAATG	426VAL	JG3	Control	I
5' AAGCAGTCATTCGCCAATG	426PHE	JG3	Mutant	I
5' GTTTGGGTAGGAGAGCCT	252GLY	JG5	Control	J
5' GTTTGGGTAAGAGAGCCT	252ARG	JG5	Mutant	J
5' CATAAGATATGAGCTGAAT	c347TYR	GL57(P)	Control	I
5' CATAAGATACGAGCTGAAT	m347TYR	GL57(P)	Mutant	I

(P): Tyr347Tyr polymorphism in UM:GL57

respectively. Algorithms that predict secondary structure such as Chou-Fasman (CF) [32] and Garnier-Osguthorpe-Robson (GOR) [33,34] provide useful tools for predicting surface features such as α-helices, β-strands, turns, or coils (ambiguous predictions). The Chou-Fasman algorithm is based on empirical rules for determining the potential of a residue to form or break α-helical and β-sheet structures based on known protein X-ray models with a tendency to underestimate α-helices and over-report β-sheet structures [32,38]. The GOR algorithm is based on the theoretical propensity of residues to form particular secondary structures based on each residue's side-chain structure and its interactions with the structure of neighboring residues [33,38]. Both GOR and Chou-Fasman algorithms assume that residues do not interact in any other way other than formation of secondary structure [39]. These methods are expected to predict α-helices and turns at approximately 70% accuracy, with an overall prediction of 50 to 65% accuracy [38,39]. Although this paper deals with potential impact of sequence change and secondary structure on nearby protein motifs, we cannot make predictions about longer range interactions or impact on interactions between protein subunits based on these analyses.

RESULTS

Evaluation of TIGR/MYOC Mutations in GLC1A Families, POAG cases, and normal controls.— Alterations in the *TIGR/MYOC* gene sequence were found by determining the entire coding sequence from affected probands in UM:JG1, UM:JG3 and UM:GL57, three families in which we had previously implicated the *GLC1A* locus in the production of juvenile glaucoma, and in an unmapped family UM:JG5 (Figure 1). For each change found by sequencing we used ASO and/or restriction enzyme digestions to determine whether that change was also present in members of the pedigree and in a panel of other JG individuals, POAG cases and normal individuals.

TIGR/MYOC missense mutations were found in all four families. In addition, polymorphisms without a corresponding change in amino acid sequence, and not co-segregating with glaucoma, were identified in UM:GL57 (codon 346) and

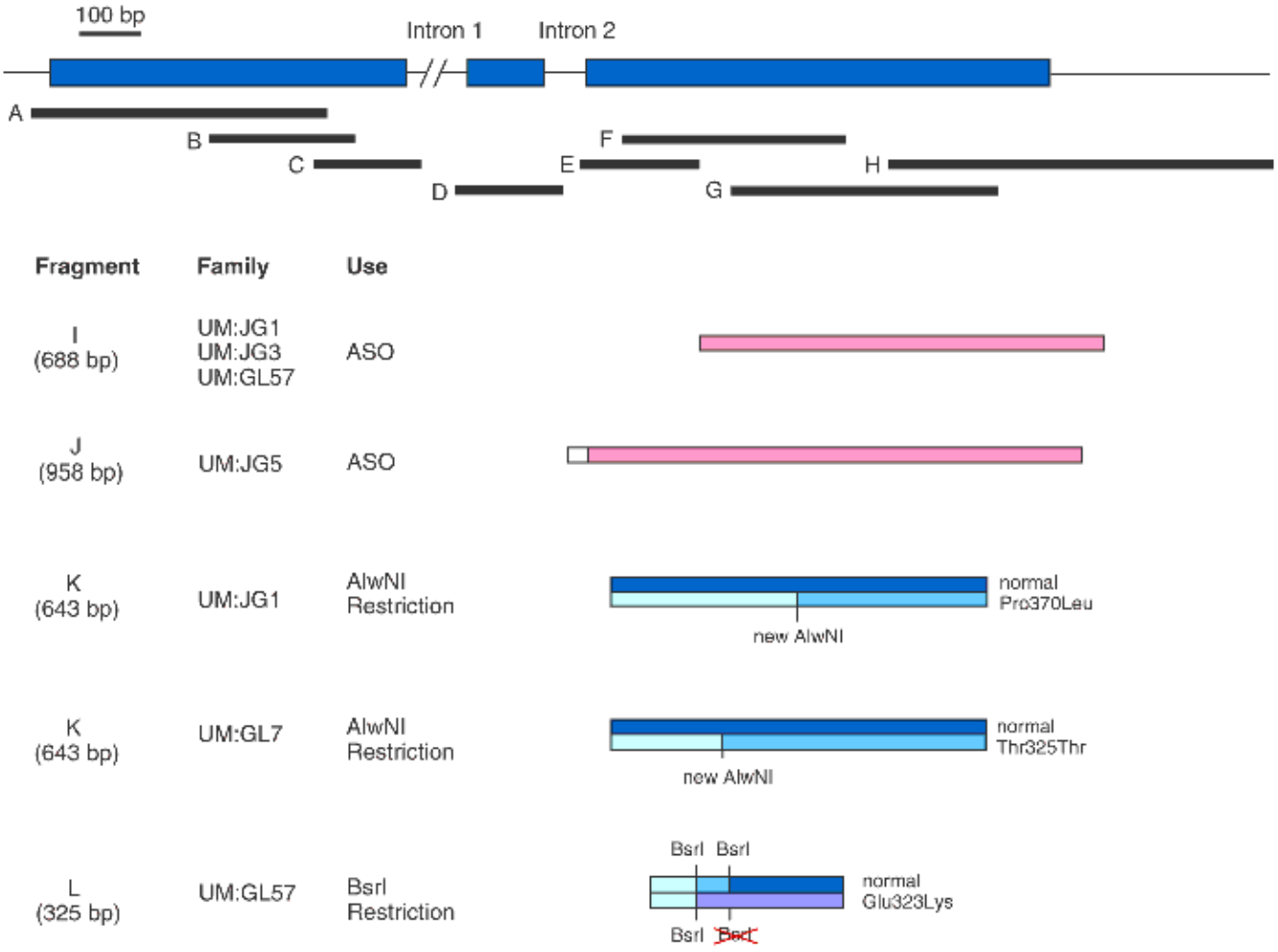

Figure 2. PCR-amplified *TIGR/MYOC* fragments used for sequencing, ASO, and restriction analysis. Gene structure of *TIGR/MYOC* is shown above with exons 1-3 in blue boxes. Fragments A-H (black boxes) were amplified by PCR using primers described in Table 1 and used as templates in subsequent DNA sequencing reactions. Fragments used for ASO (I, J) are shown by pink boxes. Fragments used for restriction analysis (K, L) to test for mutations in each family are shown as shaded blue boxes. All primers correspond to Table 1.

UM:GL7 (codon 325). The only family for which the complete coding sequence was not evaluated was UM:GL7 in which only the region surrounding the polymorphism was sequenced. No individuals were homozygous for any *TIGR/MYOC* sequence variation. The DNA sequence, restriction digestions and ASO results showed both the normal and the altered *TIGR/MYOC* base in every affected individual regardless of the mutation (Figure 3, Figure 4, and Figure 5).

A Pro370Leu mutation in *TIGR/MYOC* was identified in family UM:JG1 (Figure 3A). ASO hybridization of Fragment I (Figure 2) with labeled oligonucleotides 370Pro or 370Leu (Table 2) demonstrated co-segregation of the mutation with POAG in UM:JG1 as shown in Figure 1. The ASO results were confirmed by restriction digestion to test for the novel AlwNI restriction site (CAGNNNCTG) created by the mutation. AlwNI digestion of Fragment K produced a novel doublet of 321 and 322 bp in all affected individuals with the Pro370Leu mutation (Figure 2 and Figure 4A, lane 2). Based on combined data from AlwNI digestions and ASO hybridization, we can conclude that the UM:JG1 mutation was not present in any of the 43 normal individuals of ages 35 to 83 years (mean 55 years), 11 unrelated JG individuals with POAG diagnosed prior to age 35, nor in 43 individuals with POAG diagnosed at age 35 or later (Table 3).

During AlwNI screening for the UM:JG1 Pro370Leu mutation in the test panel, a novel polymorphism was identified in the POAG proband of family UM:GL7 (Figure 1, Table 3). AlwNI digestion of Fragment K amplified from UM:GL7 produced fragments of 450 and 193 bp (Figure 2 and Figure 4A, lane 3). Sequencing of this fragment showed a nucleotide change that does not alter the amino acid sequence at Thr325 (Figure 3B, Table 3). AlwNI digestion of Fragment K confirmed that this polymorphism is present in five out of six affected family members and in seven at risk family members (Figure 1). Prior AlwNI digestion of Fragment K to screen for the Pro370Leu mutation in UM:JG1 indicated the Thr325Thr polymorphism was also present in one 75 year old normal individual from the test panel.

The proband in family UM:JG3 was found to have a Val426Phe *TIGR/MYOC* mutation (Figure 3C). Co-segregation of the mutation with glaucoma in UM:JG3, and its absence from the JG proband and normal control panels, were demonstrated by ASO hybridization of labeled 426Phe and

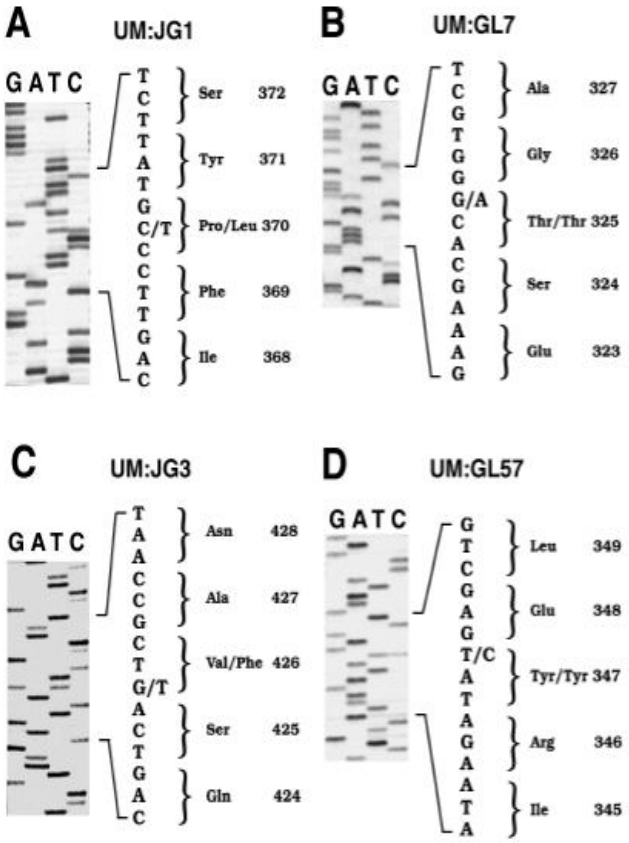

Figure 3. *TIGR/MYOC* polymorphisms in four glaucoma probands shown by autoradiography. Four nucleotide alterations in UM:JG1, UM:JG3, UM:GL57, and UM:GL7 from PCR amplified regions of *TIGR/MYOC* were sequenced as described in Materials and Methods. G, A, T, C at the top indicates the dideoxynucleotide used for each chain termination sequencing reaction. Amino acid residues encoded by each triplet are shown on the right. A. Residues 368 to 372 from the UM:JG1 proband. C/T indicates the nucleotide change resulting in the amino acid change Pro/Leu at codon 370. B. The Thr325Thr polymorphism at codon 325 in UM:GL7 results from G to A substitution. Codons 323 to 327 are shown. C. Residues 424 to 428 from the UM:JG3 proband. G/T indicates the mutation in UM:JG3 with the corresponding amino acid change Val/Phe at codon 426. D. Residues 345 to 349 from the UM:GL57 proband. T/C indicates the Tyr347Tyr polymorphism at codon 347.

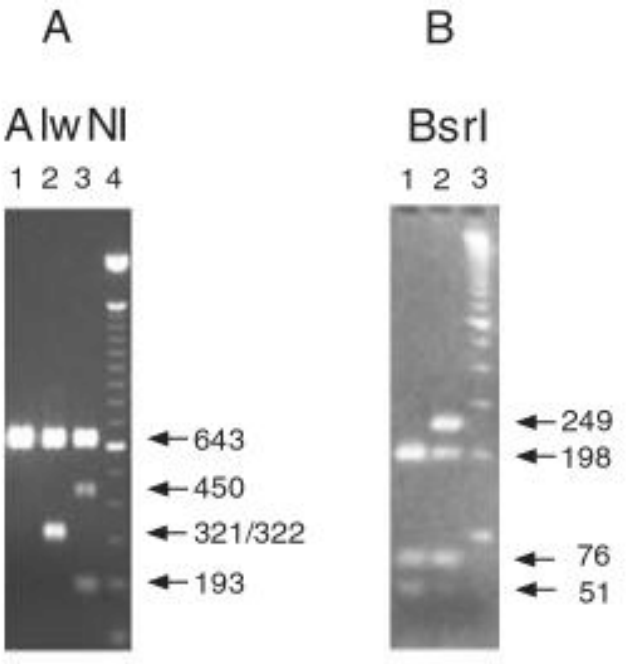

Figure 4. Heterozygous *TIGR/MYOC* sequence variants alter restriction sites. PCR-amplified fragments were digested with restriction enzymes as described in Materials and Methods. Arrows indicate fragment sizes on the right of each figure. A. Creation of new *TIGR/MYOC* exon 3 AlwNI sites in Fragment K. Lanes: 1. Unaffected control, 2. UM:JG1 proband (Pro370Leu), 3. UM:GL7 proband (Thr325Thr), 4. 100 base pair marker. B. Loss of *TIGR/MYOC* exon 3 BsrI site in Fragment L. Lanes 1. Unaffected control, 2. UM:GL57 proband (Glu323Lys), 3. 100 base pair marker.

426Val oligonucleotides to Fragment I (Figure 2, Table 2). Two previously-described individuals had borderline phenotypes in UM:JG3 with different status regarding the Val426Phe mutation. A 62 year old individual (IV-10 from reference 14) with the affected haplotype was heterozygous for the Val426Phe mutation, had IOPs of 21 and 22 mm Hg in the right and left eyes respectively, and one suspicious optic disc. The other UM:JG3 individual with a borderline phenotype is a 58 year old individual (IV-7 from reference 14) with normal haplotype, IOPs of 24 mm Hg in both eyes, and normal optic discs, who lacks the Val426Phe mutation.

A nucleotide change from GGA to AGA causes the Gly252Arg sequence variant in the UM:JG5 proband (Figure 5). It was not possible to evaluate co-segregation of the Gly252Arg variant found in family UM:JG5 since only the proband participated in the study. ASO hybridization of Fragment I (Figure 2) to 252Gly and 252Arg oligonucleotides failed to detect the Gly252Arg mutation in the JG, POAG, or normal control panels (Table 3).

Sequencing of UM:GL57 proband DNA revealed a Glu323Lys *TIGR/MYOC* mutation (Figure 5) in this family that was initially thought to contain only a silent polymorphism in *TIGR/MYOC* [40]. The Glu323Lys mutation results in the loss of one of two BsrI restriction sites (ACTGGN) in Fragment L (Figure 2). Failure of BsrI to cut at this site was used to show that the sequence change co-segregates with glaucoma in UM:GL57 (Figure 1). Digestion of Fragment L with BsrI produced fragments of 198, 76, and 51 bp in the unaffected normals while restriction fragments of 249, 198, 76, and 51 bp are produced in all individuals carrying the mutation in this family (Figure 1, Figure 2, and Figure 4B). The affected restriction pattern was not present in any DNA samples from our test panel of normal individuals, JG individuals and POAG probands (Table 3). The polymorphism initially found in the UM:GL57 proband, Tyr347Tyr, is the result of a change of TAT to TAC (Figure 3D). This polymorphism is identical to one of the four original *TIGR/MYOC* sequence variants reported by Stone et al [25]. ASO hybridization using m347Tyr and c347Tyr oligonucleotides (Table 2) to probe Fragment I (Figure 2) amplified from the members of UM:GL57 showed this polymorphism is only present in the proband and her unaffected brother, but is not present in their affected father. The lack of this polymorphism in other members of the pedigree was confirmed by determination of the DNA sequence of that region for every member of the pedigree. The Tyr347Tyr polymorphism was also present in three normal individuals, one JG proband and one POAG proband as determined by ASO or DNA sequence determination (Table 3).

Individuals in five JG families and one mixed onset family described here and previously-reported family UM:JG2 [28] all show open angles, autosomal dominant inheritance, and nearly complete penetrance (Figure 1, Table 3). When the fraction affected was plotted against age at diagnosis (Figure 6), we observed similar curves for data from UM:GL57 (Glu323Lys) and UM:JG2 (Ile477Asn). Data from UM:JG3 (Val426Phe) indicate that this mutation is associated with later onset of glaucoma relative to the early onset observed for UM:JG1 (Pro370Leu).

Motifs and secondary structure predictions for mutant forms of TIGR/MYOC— A BLAST search of GenBank identified sequence similarity between TIGR/MYOC and the

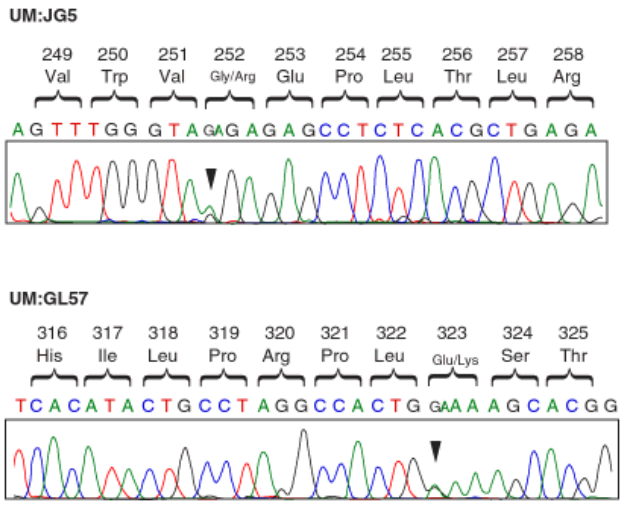

Figure 5. *TIGR/MYOC* polymorphisms in two glaucoma probands shown by dye-terminator sequencing. Chromatograms of a segment of the *TIGR/MYOC* gene containing the Gly252Arg and Glu323Lys mutations for UM:JG5 and UM:GL57, respectively. Samples were sequenced using an ABI377 semi-automated sequencer using dye-terminator chemistry. Locations of the mutated bases are shown with an arrowhead and the corresponding change in amino acid sequence is shown above.

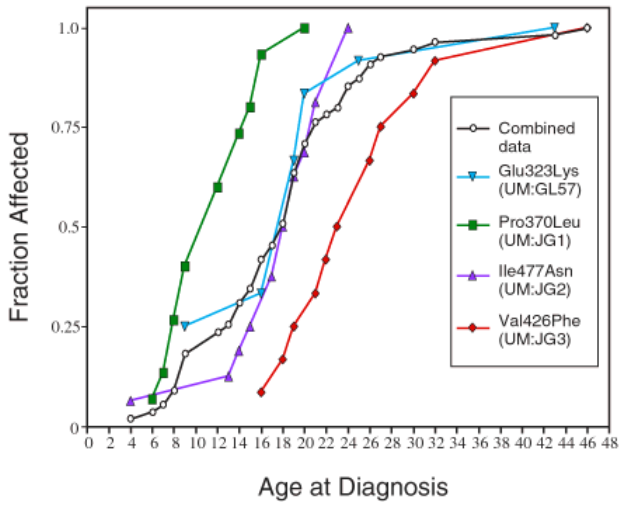

Figure 6. Fraction affected versus age at diagnosis. Only individuals with the disease phenotype are included from the pedigree. The fraction affected was calculated by dividing the running total of affected individuals by the total number of affected individuals; n = 15 for UM:JG1 (Pro370Leu), n = 16 for UM:JG2 (Ile477Asn), n = 12 for UM:JG3 (Val426Phe), n = 12 for UM:GL57 (Glu323Lys) and n = 55 for combined data. The three youngest individuals in UM:GL57 were already affected upon first examination at age 9 [30]. The green squares, blue inverted triangles, purple triangles and red diamonds indicate data from UM:JG1 (Pro370Leu), UM:GL57 (Glu323Lys), UM:JG2 (Ile477Asn), and UM:JG3 (Val426Phe), respectively. Combined data is shown by a black line with open circles.

carboxy-terminal portion of olfactomedin-like glycoproteins as noted previously [13,19,21]. Similarity was also found to the amino terminal end of rat latrophilin (LPH1/CIRL), the receptor for black widow spider neurotoxin [41,42], a seven transmembrane spanning G-protein coupled receptor that is about 1000 residues larger than TIGR/MYOC.

Predictions of protein secondary structure were performed for normal TIGR/MYOC and all mutant forms of TIGR/MYOC described in this study. Secondary structure predictions generated by the Chou-Fasman [32] and GOR [33,34] algorithms were overlaid with information on predicted potential motifs and modification sites as described in Materials and Methods (Figure 7 and Figure 8). To consider the potential importance of the reported mutations, they have been assigned to 11 groups as indicated in Figure 8. Mutations identified specifically by our group are listed in Table 3. The sources for the other mutations are indicated in the key to Figure 8. The olfactomedin homology domain covers regions 4 through 11.

Regions 1, 2, 3— Region 1 contains two mutations within the signal peptide that is cleaved to produce the 55 Kd form of the protein [15]. Minor secondary structure changes were predicted for Cys9Ser and Gln19His (Figure 9). Cys9Ser was deemed unlikely to cause glaucoma based on its occurrence in one normal individual [26]. Alward et al [26] have noted that Gln19His, which was found in one POAG proband, causes a change in charge. It is interesting to notice that this interjection of a positive charge occurs in the middle of the hydrophobic stretch of the signal peptide. The Asn73Ser substitution in region 2 was also identified in one normal individual [26] and does not alter the predicted secondary structure. Arg82Cys [26], on the other hand, introduces a turn and changes a defining residue of the predicted PKC motif (Thr-Gln-Arg) at residues 80-82 (Figure 7 and Figure 10). The Ser203Phe [26] mutation in region 3 occurs at the first residue

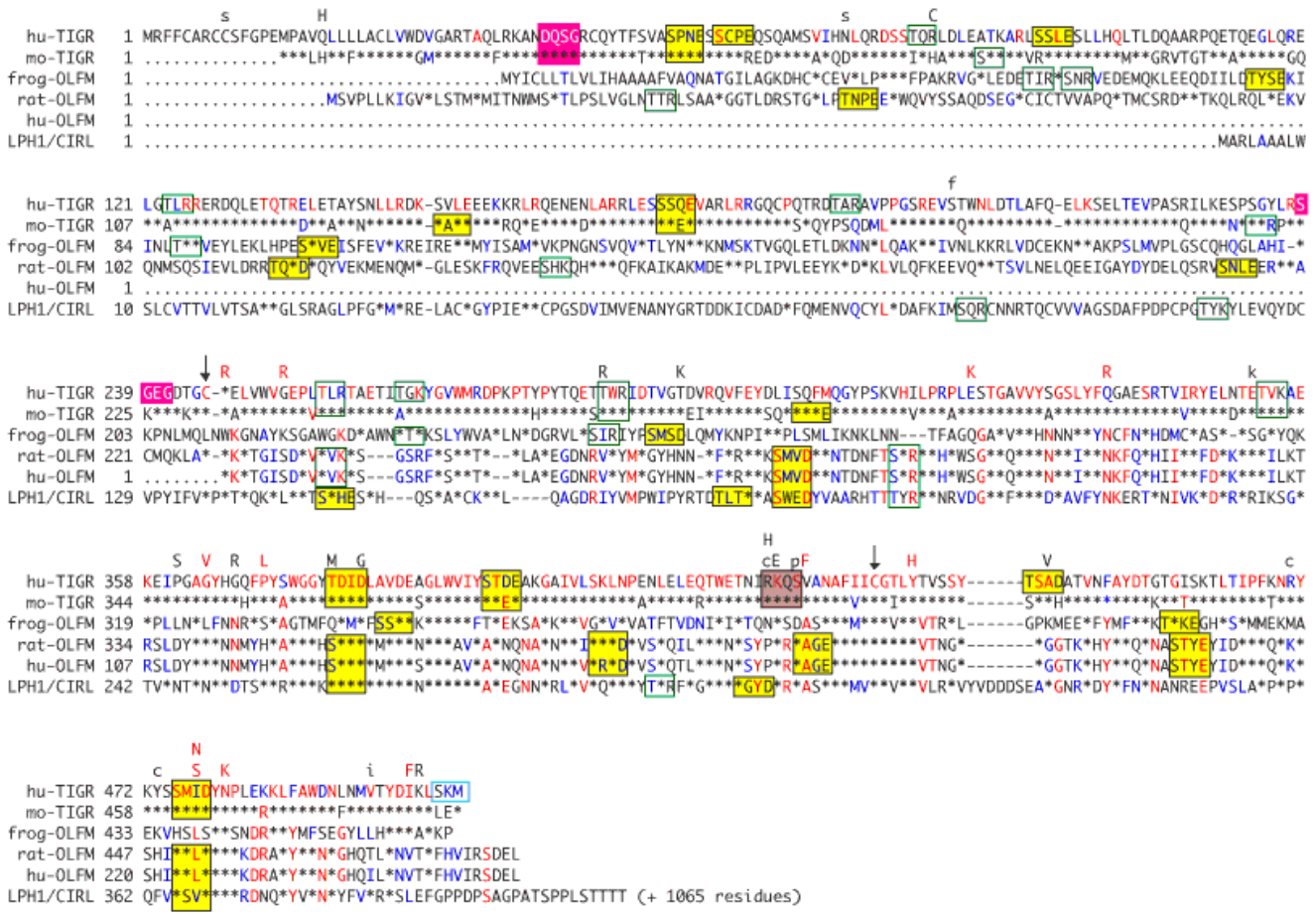

Figure 7. Amino acid alignment of olfactomedin-like proteins. Human TIGR/MYOC (hu-TIGR, U85257) [25], mouse TIGR/MYOC (mo-TIGR, AF049791, AF049792, AF049793, AF049794, AF049795, AF049796) [23,43], frog olfactomedin (frog-OLFM) (L13595) [45], rat olfactomedin-like (rat-OLFM) (U03417) [46], human olfactomedin-like (hu-OLFM) (U79299) [47], and rat latrophilin (LPH1/CIRL) (U78105) [41] proteins were compared using the PILEUP program. Amino acids are indicated by single-letter code and are numbered according to their ungapped sequence. Within the alignment, gaps introduced to optimize alignment are shown as dashes, conserved substitutions are shown in blue, highly conserved changes are shown in red, and residues identical to the human TIGR/MYOC sequence are shown by asterisks (*). The location of TIGR/MYOC missense mutations are shown above the alignment in uppercase letters. Mutations associated with juvenile-onset glaucoma are shown in red, uppercase letters. Mutations considered unlikely to cause disease by Alward et al [26] are in lowercase. Motifs identified from the Prosite database are boxed in green outline, yellow, red, gray and blue for protein kinase C, casein kinase II phosphorylation, glycosaminoglycan initiation attachment, cAMP dependent protein phosphorylation, and peroxisome C-terminal targeting signal motifs, respectively. Conserved cysteines are shown with arrows. Rat latrophilin continues an additional 1065 residues where indicated.

of the small, middle exon of TIGR/MYOC. The CF method (Figure 9) predicts a change of 15 residues from β-strand to α-helix for this mutation but these changes do not impact on nearby modification sites. This mutation was also identified in a normal individual and considered unlikely to be a disease-causing mutation [26].

Region 4— Predicted features potentially affected by sequence alterations and/or secondary structure changes in region 4 include a protein kinase C phosphorylation (PKC) site at residues 256-258 (Thr-Leu-Arg), a glycosaminoglycan

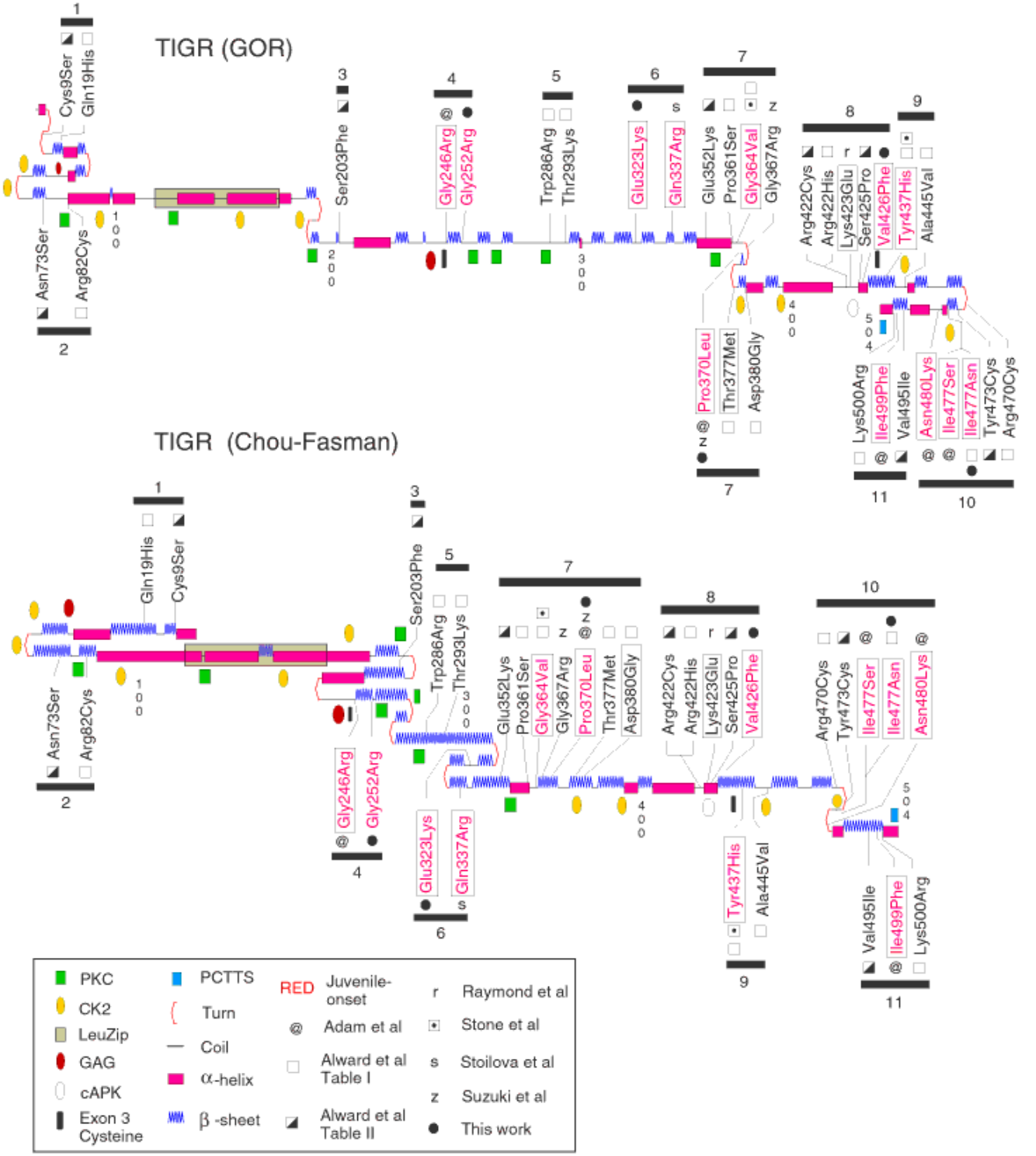

Figure 8. Locations of predicted protein modification sites and mutations on TIGR/MYOC protein. Location of 33 published TIGR/MYOC mutations superimposed on GOR (upper) and CF (lower) predictions for TIGR/MYOC. Mutations in red text are from pedigrees where the mean age at onset is under 35 years of age. Boxed mutations have been reported to co-segregate with glaucoma. Individual groups that published each mutation are shown in the key. Predicted protein modification motifs identified from Prosite and secondary structure predictions are defined in the key and correspond to the legend in Figure 7.

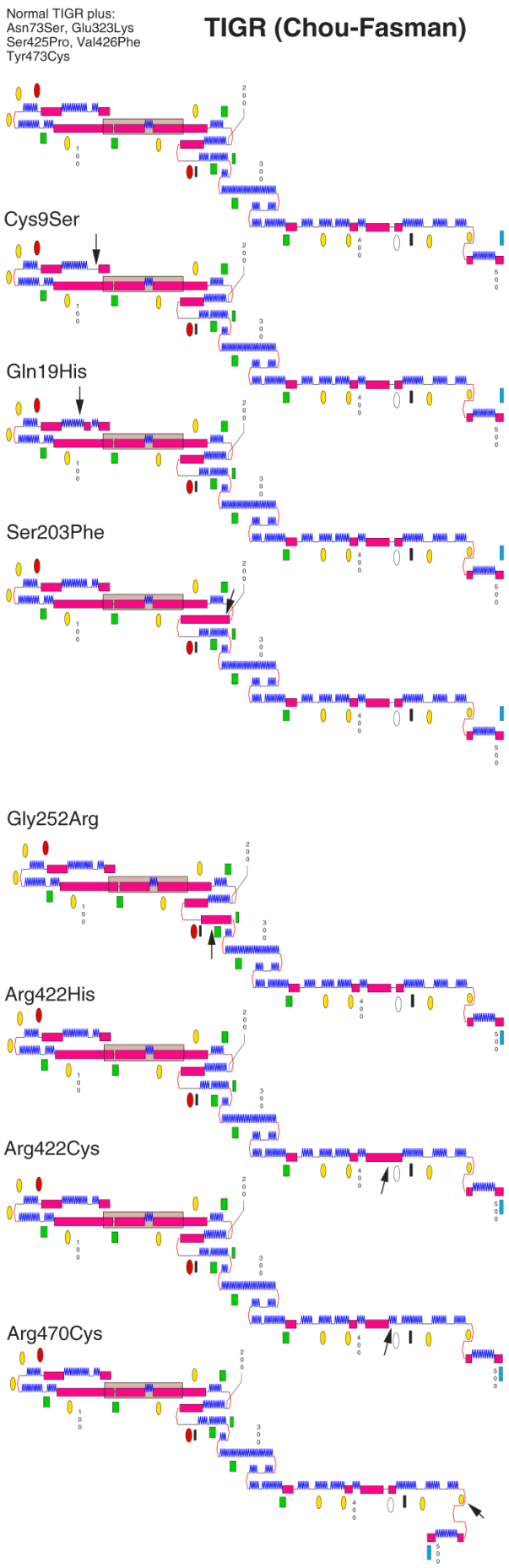

(GAG) attachment site previously predicted at residues 238-241 (Ser-Gly-Glu-Gly) [15], and a conserved cysteine (Figure 7 and Figure 8). Interestingly, the GAG attachment site is not present in the recently reported mouse ortholog [23,43] to TIGR/MYOC or in non-human members of the olfactomedin-like protein family (Figure 7). The Gly252Arg mutation in UM:JG5 (Table 3) alters the charge and is predicted by the CF algorithm to change residues 245 to 264 from β-strand to α-helix, thus altering the structure around the PKC site and Cys245 relative to normal TIGR/MYOC (Figure 7 and Figure 9). The relative conservation of Cys245 and its location on a newly created turn predicted by the GOR method (Figure 10) for the familial Gly246Arg mutation [22] raises questions about the role of conserved cysteines in normal TIGR/MYOC function.

Region 5— The Trp286Arg and Thr293Lys mutations described by Alward et al [26] fall near a predicted PKC site (Thr-Trp-Arg) at residues 285-287 (Figure 7 and Figure 8). The Trp286Arg mutation changes both the charge and polarity and is predicted to induce β-strand formation within the PKC site while the Thr293Lys mutation inserts an extra turn into the structure (Figure 10).

Region 6— Unlike the other mutations described in this work, the Glu323Lys (UM:GL57) mutation occurs in a relatively non-conserved region of olfactomedin-like proteins and there is no evident basis for its impact on predicted protein modification sites (Figure 7). The mutation results in a net plus 2 change in charge but had no predicted alteration in

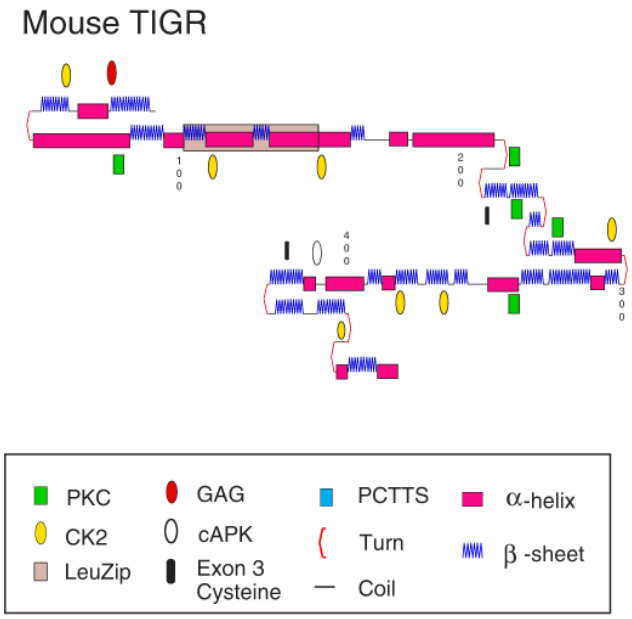

Figure 9. Chou-Fasman analysis of mutations altering TIGR/MYOC predicted secondary structure and protein modification sites. CF predictions for TIGR/MYOC containing Cys9Ser, Gln19His, Ser203Phe, Gly252Arg, Arg422His, Arg422Cys, and Arg470Cys mutations. In addition, the prediction for mouse TIGR/MYOC is shown below. Mutations are indicated by arrows. Symbols for protein modification sites and secondary structure are defined in the key shown above.

secondary structure using both algorithms (Table 3). A turn is predicted by the GOR method for the Gln337Arg mutation [29] (Figure 10). However, both these familial mutations and the predicted structural change are not located near a protein modification site.

Region 7— The UM:JG1 mutation (Pro370Leu) is one of several reported mutations clustered on a predicted double turn in region 7 (Figure 8, Table 3). A nearby casein kinase II phosphorylation (CK2) motif was conserved as Thr-Asp-Ile-Asp across the mammalian members of this group at residues 377-380 (Figure 7). Accessibility to the phosphorylation substrate, Thr377, may be altered since one of two closely connected turns is lost near the CK2 site (Figure 10). Six additional mutations have been reported near this same CK2 site. One of these, Pro361Ser [26], is predicted to have a secondary structure similar to Pro370Leu, which would make a comparison of clinical features between these two families intriguing (Figure 10). The Glu352Lys mutation [26] alters the charge adjacent to a predicted PKC site at residues 353-355 (Figure 7); however this mutation makes only minor changes in the secondary structure prediction (Figure 10) and was considered by the authors to be unlikely to cause disease [26]. The previously reported Gly364Val [25,26] and Gly367Arg [27] mutations alter the polarity and charge, respectively and have a more subtle effect on the predicted turn shown in Figure 10, with unknown consequences to the neighboring CK2 site. The predicted secondary structure for the Thr377Met [26] mutation is identical to that of Gly364Val, but also changes the polarity and the putative phosphorylation substrate itself, presumably eliminating phosphorylation at the CK2 site (Figure 10). The Asp380Gly mutation [26] changes the GOR prediction at one residue (from α-helix to β-strand) but of more interest, eliminates one of the acidic determinants that define the CK2 motif (Figure 7). Although these data suggest that phosphorylation of Thr377 at the CK2 site is important to normal TIGR/MYOC function, a substantial difference in age at onset for the Pro370Leu (Table 3) and Thr377Met [26] mutations suggests that the Pro370Leu conformation change may be bringing about more than just a failure of CK2 modification.

Region 8— A region for which the CF and GOR algorithms both predict similar secondary structures (Figure 8) contains five mutations. This region also contains a predicted cAMP-dependent protein kinase (cAPK) site for both human and mouse TIGR/MYOC at residues 422-425 with Ser425 as the phosphorylation substrate (Figure 7). Analysis of the Val426Phe (UM:JG3) mutation failed to produce any predicted secondary structure alterations by either the GOR or Chou-Fasman algorithms. However, it does interject an aromatic ring immediately adjacent to the predicted cAPK site (Arg-Lys-Gln-Ser) (Figure 7). Three recently characterized mutations described by Alward et al [26]-Arg422His, Arg422Cys, and Ser425Pro-also fall within this cAPK site but only Arg422His was judged to be a disease-causing mutation. It is unclear if the structural changes alone for the Arg422His and Arg422Cys mutations would effect phosphorylation at the cAPK site (Figure 9). Alward and colleagues predicted that Ser425Pro and Arg422Cys were unlikely to cause disease because each one was detected in one out of 505 individuals from the general (unexamined) population [26]. However, Ser425Pro eliminates the proposed phosphorylation substrate (Figure 7) while Arg422Cys is predicted both to alter the protein structure and to change one of the defining basic residues of the cAPK motif (Figure 7 and Figure 9). Thus, although these analyses do not prove that the predicted cAPK motif is used, the benign nature of these sequence changes does not seem assured. The familial

TABLE 3. CO-SEGREGATION AND PREDICTED PROTEIN CHANGES IN SEVEN *TIGR* MUTATIONS

Mutation Identified in Pedigree Proband	Gly252Arg	Glu323Lys	Tyr347Tyr	Thr325Thr	Pro370Leu	Val426Phe	Ile477Asn
Pedigree	UM:JG5	UM:GL57	UM:GL5	UM:GL7	UM:JG1	UM:JG3	UM:JG2
Fraction of affected family members with mutation	1/1	11/11	1/1	5/5	15/15	12/12	15/15
Co-Segregation?	ND	Yes	No	No	Yes	Yes	Yes
Fraction of examined normals with mutation	0/43	0/43	3/43	1/43	0/43	0/43	0/48
Changes in charge	+1	+2	NA	NA	None	None	None
Structure changes	Strand to helix (CF)	None	NA	NA	Loss of turn (GOR)	None	Gain of turn (GOR)
Motifs near mutation	GAG (238-241)	None	None	None	CK2 (377-380)	cAPK (422-425)	CK2 (475-478)
	PKC (256-258)						
Source	This work	This work	This work	This work	This work	This work	Ref. 28

—

ND: Not determined; NA:Not applicable; GOR: Garnier-Osguthorpe-Robson; CF: Chou-Fasman algorithm; CK2: Casien kinase II phosphorylation site; cAPK: cAMP-dependent protein kinase phosphorylation site; PKC: Protein kinase C phosphorylation site; GAG: Glycosaminoglycan initiation site.

Figure 10. Legend next page.

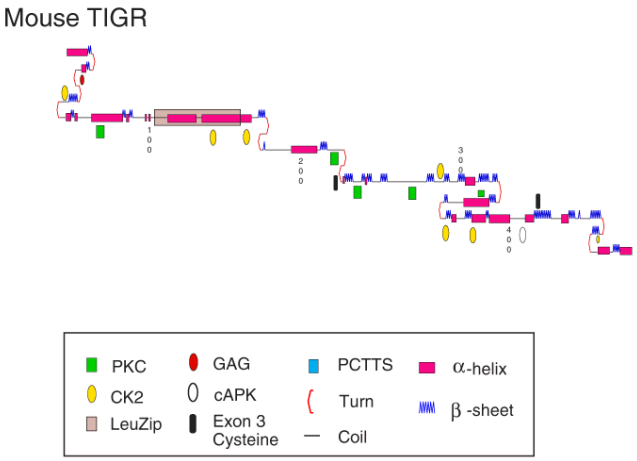

Figure 10 (continued). Garnier-Osguthorpe-Robson analysis of mutations altering TIGR/MYOC predicted secondary structure and protein modification sites. GOR predictions for TIGR/MYOC containing Arg82Cys, Gly246Arg, Trp286Arg, Thr293Lys, Gln337Arg, Glu352Lys, Pro361Ser, Gly364Val, Gly367Arg, Pro370Leu, Thr377Met, Tyr437His, Ala445Val, Ile477Asn, Ile477Ser, Asn480Lys, Ile499Phe, and Lys500Arg mutations, in addition to mouse TIGR/MYOC below. Mutations are indicated by arrows. Symbols for protein motifs and structural predictions are defined in the key shown above.

Lys423Glu mutation [44] involves a minus 2 change in charge within this basic cAPK motif (Figure 7 and Figure 8), reinforcing the idea that phosphorylation at this site plays a role in the normal function of TIGR/MYOC. Region 8 also contains an entirely conserved cysteine at residue 433 (Figure 7 and Figure 8). Based on the model for the formation of olfactomedin multimers [45], Nguyen et al [15] proposed that cysteine-cysteine bonds and formation of intermolecular leucine zippers contribute to the formation of high molecular weight TIGR/MYOC multimers. Until further experimental evidence is available to elaborate on the formation of these multimers, the impact of TIGR/MYOC mutations on formation of disulfide bonds that include Cys433 remains unknown. It is interesting to note that none of the mutations so far reported eliminate the conserved TIGR/MYOC cysteines.

Region 9— A CK2 motif at residues 443-446 (Thr-Ser-Ala-Asp) is potentially affected by two mutations in region 9 (Figure 7). The Tyr437His [25,26] and Ala445Val [26] mutations both make small changes in the GOR prediction for TIGR/MYOC at this motif but provide no apparent basis for effect on the neighboring conserved Cys433 (Figure 10).

Region 10— A single turn (GOR) or a double turn (CF) is predicted near a CK2 motif (Ser-Met-Ile-Asp) at residues 475-478 (Figure 7 and Figure 8), with Ser475 as the expected phosphorylation substrate. Three of the mutations in this region co-segregate with the juvenile-onset form of glaucoma. The Ile477Asn [26,28] and Ile477Ser [22] mutations each introduce an extra turn into the GOR prediction for TIGR/MYOC, perhaps modifying the organization of the carboxy terminal region. Of the two mutations, Ile477Asn (Table 3) seems to result in earlier onset of glaucoma with an average age at diagnosis approximately 10 years earlier than Ile477Ser [22,26,28]. The Arg470Cys mutation [26] adds a turn at the CK2 motif in the CF prediction (Figure 9), while Tyr473Cys [26] does not alter the predicted structure using either method. Asn480Lys [22] induces a change from an unspecified coil to an α-helix in close proximity to the CK2 motif in addition to altering the charge (Figure 10).

Region 11— The carboxy terminus in region 11 ends with a tripeptide (Ser-Lys-Met) C-terminal peroxisome targeting signal (PCTTS) not present in mouse TIGR/MYOC nor other TIGR/MYOC-like proteins (Figure 7 and Figure 8) [23,43]. Although the Ile499Phe [25] and Lys500Arg [26] mutations do not directly change the PCTTS sequence, they do make minor changes in the secondary structure at the carboxy terminus (Figure 10). Although there are indications of TIGR/MYOC export from cultured TM cells [15,16] and native TM cells in subjects with glaucoma [24], the predicted peroxisomal targeting signal suggests intracellular trafficking that raises questions about the role of TIGR/MYOC within the normal cell.

DISCUSSION

This study resulted in the identification of *TIGR/MYOC* mutations Pro370Leu, Val426Phe, and Glu323Lys as the apparent causes of glaucoma in three previously reported *GLC1A* glaucoma families, UM:JG1, UM:JG3, and UM:GL57, respectively. *TIGR/MYOC* missense mutation Gly252Arg was found in family UM:JG5, which is too small to allow evaluation of co-segregation. Like most *TIGR/MYOC* missense mutations previously noted by others [22,25-29], these mutations all occur in the third exon, which shares significant homology to several olfactomedin-like proteins (Figure 7). The regions of homology shared between TIGR/MYOC and olfactomedin-like glycoproteins with different overall structure suggest that the olfactomedin domain defines a functional motif that can occur in different protein contexts. This is particularly evident in LPH1/CIRL, a plasma membrane-bound G protein-coupled receptor whose large amino terminal extracellular domain contains an olfactomedin-like domain. It is not yet known whether the different olfactomedin-related proteins share related functions.

Comparison of age at onset in four of our *GLC1A* families helped us to demonstrate that an especially severe, early-onset form of glaucoma results from the Pro370Leu mutation found in UM:JG1, a family in which no cases of non-penetrance have been observed (Figure 6). It is interesting to note that this same mutation appears to cause a similar early-onset form of glaucoma in two French families [22] and in a Japanese family [27].

Novel mutation Val426Phe apparently causes a later onset of glaucoma in a family in which a case of reduced penetrance has been observed. One member of UM:JG3 with a borderline phenotype is heterozygous for the Val426Phe mutation. Thus, this case of substantially reduced penetrance cannot be explained by the model of homoallelic complementation proposed by Raymond and colleagues [44] to explain normal phenotypes in individuals homozygous for *TIGR/MYOC* mutations. The reason for incomplete penetrance of the

glaucoma phenotype in this individual remains unknown. Another individual in the UM:JG3 pedigree had elevated IOP but lacked the Val426Phe *TIGR/MYOC* mutation. We conclude that the ocular hypertension (OHT) in this individual is due to a different, as yet unknown, underlying cause and not related to the OHT associated with glaucoma in other members of this family.

The Glu323Lys *TIGR/MYOC* mutation that appears to cause juvenile glaucoma in UM:GL57 was not the only *TIGR/MYOC* sequence change found in this family. A Tyr347Tyr polymorphism was identified on the copy of chromosome 1 that does not contain the Glu323Lys mutation and does not appear to be a cause of glaucoma in UM:GL57. Similarly, a Thr325Thr variant found in UM:GL7 appears unlikely to cause disease, but we cannot rule out the presence of a causative mutation on unsequenced portions of either copy of *TIGR/MYOC*.

The Gly252Arg sequence variant in the UM:JG5 proband is the most problematic of the sequence variants we detected in this study. Due to insufficient sample size, we could not use information on co-segregation to help confirm a causative role for this mutation. The Gly252Arg variant was not identified in any other families in our panel of glaucoma probands, has not been reported by others, and was also not found in our panel of normal controls. Since this sequence variant is so rare, we do not yet know whether it is causative; however, it must be noted that Gly252Arg does cause a change in charge and an alteration to the secondary structure in the immediate vicinity of a predicted phosphorylation site. Because these findings are not conclusive, caution will be needed in offering any interpretation of these testing results to individuals in whom Gly252Arg is detected. This difficulty with interpretation of the possible causative role of a sequence variant is encountered more frequently in cases of *TIGR/MYOC* sequence variants found in adult-onset glaucoma cases where small numbers of affected individuals from any one family often prevent evaluation of co-segregation of mutation and disease [26].

Our data offer predictions of how *TIGR/MYOC* mutations may be altering normal TIGR/MYOC structure and function. Alteration of secondary structure, as we predict for many of the 33 TIGR/MYOC amino-acid substitutions analyzed here, is one obvious mechanism by which missense mutations may act. Our analyses of these mutations also make additional, more precise predictions regarding the importance of predicted casein kinase 2 sites at Thr377 and Ser475, a predicted cAMP-dependent protein kinase site at Ser425, and a potential trafficking sequence in the carboxy terminal region of the protein. Due to the limited predictive power of the algorithms, these analyses cannot predict that glaucoma will actually result from any given mutation. However, our results do provide a useful framework to both direct further studies and to interpret findings of rare novel sequence variants such as Gly252Arg and Ser425Pro, where efforts to interpret mutation screening results are confounded by lack of co-segregation information and by the possibility of later development of glaucoma in apparently normal individuals. Until we have functional assays and a better understanding of TIGR/MYOC function, it is especially important that great caution be exercised when counseling individuals who carry very rare polymorphisms judged to be benign because they have only been found in the general population.

ACKNOWLEDGEMENTS

This study was supported in part by grants EY09580 (JER), EY07003 (CORE), EY08905 (TN), EY02477 (JP) from the National Eye Institute, Bethesda, Maryland, by an unrestricted grant from Research to Prevent Blindness, Inc., New York, New York, by the Glaucoma Research Foundation, San Francisco, CA, and by the Helen Van Arnam Glaucoma Research Fund of the University of Michigan Department of Ophthalmology.

REFERENCES

1. Sheffield VC, Stone EM, Alward WL, Drack AV, Johnson AT, Streb LM, Nichols BE. Genetic linkage of familial open angle glaucoma to chromosome 1q21-q31. Nat Genet 1993; 4:47-50.

2. Stoilova D, Child A, Trifan OC, Crick RP, Coakes RL, Sarfarazi M. Localization of a locus (GLC1B) for adult-onset primary open angle glaucoma to the 2cen-q13 region. Genomics 1996; 36:142-150.

3. Wirtz MK, Samples JR, Kramer PL, Rust K, Topinka JR, Yount J, Koler RD, Acott TS. Mapping a gene for adult-onset primary open-angle glaucoma to chromosome 3q. Am J Hum Genet 1997; 60:296-304.

4. Trifan OC, Traboulsi EI, Stoilova D, Alozie I, Nguyen R, Raja S, Sarfarazi M. A third locus (GLC1D) for adult-onset primary open-angle glaucoma maps to the 8q23 region. Am J Ophthalmol 1998; 126:17-28.

5. Sarfarazi M, Child A, Stoilova D, Brice G, Desai T, Trifan OC, Poinoosawmy D, Crick RP. Localization of the fourth locus (GLC1E) for adult-onset primary open-angle glaucoma to the 10p15-p14 region. Am J Hum Genet 1998; 62:641-652.

6. Wirtz MK, Samples JR, Kramer PL, Yount J, Rust K, Acott TS. Identification of a new adult-onset primary open-angle glaucoma locus - GLC1F. Invest Ophthalmol Vis Sci 1998; 39:S512.

7. Richards JE, Lichter PR, Boehnke M, Uro JL, Torrez D, Wong D, Johnson AT. Mapping of a gene for autosomal dominant juvenile-onset open-angle glaucoma to chromosome 1q. Am J Hum Genet 1994; 54:62-70.

8. Wiggs JL, Haines JL, Paglinauan C, Fine A, Sporn C, Lou D. Genetic linkage of autosomal dominant juvenile glaucoma to 1q21-q31 in three affected pedigrees. Genomics 1994; 21:299-303.

9. Meyer A, Valtot F, Bechetoille A, Rouland JF, Dascotte JC, Ferec C, Bach JF, Chaventre A, Garchon HJ. [Linkage between juvenile glaucoma and chromosome 1q in 2 French families]. C R Acad Sci III 1994; 317:565-570. French.

10. Morissette J, Cote G, Anctil JL, Plante M, Amyot M, Heon E, Trope GE, Weissenbach J, Raymond V. A common gene for juvenile and adult-onset primary open-angle glaucomas confined on chromosome 1q. Am J Hum Genet 1995; 56:1431-1442.

11. Graff C, Urbak SF, Jerndal T, Wadelius C. Confirmation of linkage to 1q21-31 in a Danish autosomal dominant juvenile-onset glaucoma family and evidence of genetic heterogeneity. Hum Genet 1995; 96:285-289.

12. Raymond V. Molecular genetics of the glaucomas: mapping of the first five "GLC" loci. Am J Hum Genet 1997; 60:272-277.

13. Sarfarazi M. Recent advances in molecular genetics of glaucoma. Hum Mol Genet 1997; 6:1667-1677.

14. Johnson AT, Richards JE, Boehnke M, Stringham HM, Herman SB, Wong DJ, Lichter PR. Clinical phenotype of juvenile-onset primary open-angle glaucoma linked to chromosome 1q. Ophthalmology 1996; 103:808-814.

15. Nguyen TD, Chen P, Huang WD, Chen H, Johnson D, Polansky JR. Gene structure and properties of TIGR, an olfactomedin-related glycoprotein cloned from glucocorticoid-induced trabecular meshwork cells. J Biol Chem 1998; 273:6341-6350.

16. Polansky JR, Fauss DJ, Chen P, Chen H, Lutjen-Drecoll E, Johnson D, Kurtz RM, Ma ZD, Bloom E, Nguyen TD. Cellular pharmacology and molecular biology of the trabecular meshwork inducible glucocorticoid response gene product. Ophthalmologica 1997; 211:126-139

17. Polansky JR, Nguyen TD. The *TIGR* gene, pathogenic mechanisms, and other recent advances in glaucoma genetics. Current Opinions in Ophthalmology 1998; 9:15-23.

18. Nguyen TD, Huang WD, Bloom E, Polansky JR. Glucocorticoid effects on HTM cells: molecular biology approaches. In: Lutjen-Drecoll E, editor. Basic aspects of glaucoma research III. Stuttgart: Schattauer; 1993. p. 331-343.

19. Kubota R, Noda S, Wang Y, Minoshima S, Asakawa S, Kudoh J, Mashima Y, Oguchi Y, Shimizu N. A novel myosin-like protein (myocilin) expressed in the connecting cilium of the photoreceptor: molecular cloning, tissue expression, and chromosomal mapping. Genomics 1997; 41:360-369.

20. Kubota R, Kudoh J, Mashima Y, Asakawa S, Minoshima S, Hejtmancik JF, Oguchi Y, Shimizu S. Genomic organization of the human myocilin gene (MYOC) responsible for primary open angle glaucoma (GLC1A). Biochem Biophys Res Commun 1998; 396-400.

21. Ortego J, Escribano J, and Coca-Prados M. Cloning and characterization of subtracted cDNAs from a human ciliary body library encoding TIGR, a protein involved in juvenile open angle glaucoma with homology to myosin and olfactomedin. FEBS Lett 1997; 413:349-353.

22. Adam MF, Belmouden A, Binisti P, Brezin AP, Valtot F, Bechetoille A, Dascotte JC, Copin B, Gomez L, Chaventre A, Bach JF, Garchon HJ. Recurrent mutations in a single exon encoding the evolutionarily conserved olfactomedin-homology domain of TIGR in familial open-angle glaucoma. Hum Mol Genet 1997; 6:2091-2097.

23. Fingert JH, Ying L, Swiderski RE, Nystuen AM, Arbour NC, Alward WL, Sheffield VC, Stone EM. Characterization and comparison of the human and mouse GLC1A glaucoma genes. Genomic Res 1998; 8:377-384.

24. Lutjen-Drecoll E, May CA, Polansky JR, Johnson DH, Bloemendal H, Nguyen TD. Localization of the stress proteins α B-crystallin and trabecular meshwork inducible glucocorticoid response protein in normal and glaucomatous trabecular meshwork. Invest Ophthalmol Vis Sci 1998; 39:517-525.

25. Stone EM, Fingert JH, Alward WLM, Nguyen TD, Polansky JR, Sunden SLF, Nishimura D, Clark AF, Nystuen A, Nichols BE, Mackey DA, Ritch R, Kalenak JW, Craven ER, Sheffield VC. Identification of a gene that causes primary open angle glaucoma. Science 1997; 275:668-670.

26. Alward WL, Fingert JH, Coote MA, Johnson AT, Lerner SF, Junqua D, Durcan FJ, McCartney PJ, Mackey DA, Sheffield VC, Stone EM. Clinical features associated with mutations in the chromosome 1 open-angle glaucoma gene. N Eng J Med 1998; 338:1022-1027.

27. Suzuki Y, Shirato S, Taniguchi F, Ohara K, Nishimaki K, Ohta S. Mutations in TIGR gene in familial primary open-angle glaucoma in Japan. Am J Hum Genet 1997; 61:1202-1204.

28. Richards JE, Ritch R, Lichter PR, Rozsa FW, Stringham HM, Caronia RM, Johnson D, Abundo GP, Willcockson J, Downs CA, Thompson DA, Musarella MA, Gupta N, Othman MI, Torrez DM, Herman SB, Wong DJ, Higashi M, Boehnke M. Novel trabecular meshwork inducible glucocorticoid response mutation in an eight-generation juvenile-onset primary open-angle glaucoma pedigree. Ophthalmology 1998; 105:1698-1707.

29. Stoilova D, Child A, Brice G, Crick RP, Fleck BW, Sarfarazi M. Identification of a new 'TIGR' mutation in a family with juvenile-onset primary open angle glaucoma. Ophthalmic Genet 1997; 18:109-118.

30. Lichter PR, Richards JE, Boehnke M, Othman M, Cameron BD, Stringham HM, Downs CA, Lewis SB, Boyd BF. Juvenile glaucoma linked to the GLC1A gene on chromosome 1q in a Panamanian family. Am J Ophthalmol 1997; 123:413-416.

31. Bolton ET, McCarthy BJ. A general method for the isolation of RNA complementary to DNA. Proc Natl Acad Sci U S A 1962; 48:1390.

32. Chou PY, Fasman GD. Prediction of protein conformation. Biochemistry 1974; 13:222-245.

33. Garnier J, Osguthorpe DJ, Robson B. Analysis of the accuracy and implications of simple methods for predicting the secondary structure of globular proteins. J Mol Biol 1978; 120:97-120.

34. Garnier J, Gibrat JF, Robson B. GOR method for predicting protein secondary structure from amino acid sequence. Methods Enzymol 1996; 266:540-553.

35. Henikoff S, Henikoff JG. Protein family classification based on searching a database of blocks. Genomics 1994; 19:97-107.

36. Attwood TK, Avison H, Beck ME, Bewley M, Bleasby AJ, Brewster F, Cooper P, Degtyarenko K, Geddes AJ, Flower DR, Kelly MP, Lott S, Measures KM, Parry-Smith DJ, Perkins DN, Scordis P, Scott D, Worledge C. The PRINTS database of protein fingerprints: a novel information resource for computational molecular biology. J Chem Inf Comput Sci 1997; 37:417-424.

37. Bairoch A, Bucher P, Hofmann K. The PROSITE database, its status in 1997. Nucleic Acids Res 1997; 25:217-221.

38. Nishikawa K. Assessment of secondary-structure prediction of proteins. Comparison of computerized Chou-Fasman method with others. Biochim Biophys Acta 1983; 748:285-299.

39. Strelets VB. New machine learning technique for analysis and prediction of sequence and structure features: protein secondary structure prediction. Network Science 1995; 1(4) <http://www.netsci.org/Science/Bioinform/feature03.html>.

40. Rozsa FW, Ritch R, Othman M, Lichter PR, Johnson AT, Shimizu S, Downs CA, Nguyen TD, Caronia RM, Johnson D, Abundo GP, Musarella MA, Gupta N, Polansky J, Richards JE. GLC1A

glaucoma family lacks mutations in coding sequences or splice sites of the *TIGR* glaucoma gene. Invest Ophthalmol Vis Sci 1998; 39:S32.

41. Davletov BA, Shamotienko OG, Lelianova VG, Grishin EV, Ushkaryov YA. Isolation and biochemical characterization of a Ca2+-independent alpha-latrotoxin-binding protein. J Biol Chem 1996; 271:23239-23245.

42. Lelianova VG, Davletov BA, Sterling A, Rahman MA, Grishin EV, Totty NF, Ushkaryov YA. Alpha-latrotoxin receptor, latrophilin, is a novel member of the secretin family of G protein-coupled receptors. J Biol Chem 1997; 272:21504-21508.

43. Abderrahim H, Jaramillo-Babb VL, Zhou Z, Vollrath D. Characterization of the murine TIGR/myocilin gene. Mamm Genome 1998; 9:673-675

44. Raymond V, Clepet C, Dubois S, Moisan S, Winstall E, Vermeeren D, Plante M, Cote G, Anctil JL, Amyot M, Nguyen TD, Polansky J, Falardeau P, Morissette J. Identification of unaffected homozygotes for primary open-angle glaucoma caused by the *TIGR* gene: evidence for a new form of dominance in man. Invest Ophthalmol Vis Sci 1998; 39:S688.

45. Yokoe H, Anholt RR. Molecular cloning of olfactomedin, an extracellular matrix protein specific to olfactory neuroepithelium. Proc Natl Acad Sci U S A. 1993; 90:4655-4659.

46. Danielson PE, Forss-Petter S, Battenberg EL, deLecea L, Bloom FE, Sutcliffe JG. Four structurally distinct neuron-specific olfactomedin-related glycoproteins produced by differential promoter utilization and alternative mRNA splicing from a single gene. J Neurosci Res 1994; 38:468-478.

47. Andersson B, Wentland MA, Ricafrente JY, Liu W, Gibbs RA. A “double adaptor” method for improved shotgun library construction. Anal Biochem 1996; 236:107-113.